



Improvements in the Modelling of Micro Fission Chambers Operated in Current Mode

Sébastien P. Chabod, Alain Letourneau

Abstract—We recall the theoretical bases necessary to model micro fission chambers operated in current mode. For these detectors, we propose formulae for the lower and upper limits of the saturation zone, obtained through analytical and numerical resolutions of the charge transport equations. Using these results, we calculate the voltage extension of the saturation plateau, as function of parameters such as the electrode geometries or the characteristics of the filling gas.

Index Terms—Ionization detector, fission chamber, current mode, saturation curve

I. INTRODUCTION

Fission chambers are ionization detectors designed to carry out on-line neutron flux measurements. They comprise two parallel electrodes separated by a filling gas, generally pure argon at atmospheric pressures. As the chambers are used to detect neutrons, their anode is usually coated with a fissile element. Under irradiation, incident neutrons induce nuclear fissions inside the anode deposit, generating two high energy fission products emitted in opposite directions. One is absorbed in the anode; the other crosses the inter-electrode space ionizing the filling gas on its wake. The electric charges generated can then be collected if a voltage is applied at the electrodes.

When the ambient neutron flux is low, fission chambers are used in pulse mode, where fissions are counted event by event. For intermediate neutron fluxes, the detectors can be used in Campbelling mode (or MSV mode). However, when the neutron flux reaches high levels, the event pile-up induced by the high fission rate requires a current mode acquisition. The monitoring of the current as a function of the voltage applied at the electrodes gives a characteristic curve, referred as the calibration curve. This curve presents a saturation plateau, where the current delivered is proportional to the neutron flux while remaining independent of the voltage. Consequently, fission chambers used in current mode are generally operated within the voltage limits of the saturation regime.

To conduct their measurements, the fission chamber users must identify these reference voltages, needed for their

detectors to achieve saturation. The voltages depend on a number of parameters, which include the neutron flux value, but also the geometry or filling gas characteristics of the detector. As a result, they are currently obtained through calibration experiments, using neutron sources such as research reactors. As the calibration procedures are carried out in irradiated environments, they require a constraining logistic as well as sizeable financial, time or human resources. Above all, they have to be reinitialized each time the detector's characteristics are modified.

To cut costs and accelerate production, fission chamber conception should no longer rely on sole empirical studies. As other technological products now, their design can profit from simulation studies, aiming to predict the behaviour of the detectors in the widest range of irradiation conditions possible. For a better predictability, the simulations should include physical models, whose description is the goal of this paper. In section 2, we summarize the main physical processes at work inside the fission chambers. In section 3, we estimate and optimize the voltage extension of the saturation plateau, before concluding.

II. SUMMARY OF THE MAIN PHYSICAL PROCESSES AT WORK INSIDE A FISSION CHAMBER

Fission chambers operated in high neutron fluences are filled with rare gases, as these non-molecular elements do not deteriorate through radiation induced dissociation reactions. Furthermore, their gas pressures seldom exceed one bar. Higher values increase the risk of filling gas escape in the irradiation device (along with radioactive gaseous fission products), and are no longer needed since the number of electric charges generated in the detector due to the high fission rate is large enough to ensure measurable signals. Consequently, in this paper we focus on cylindrical chambers filled with rare gases at atmospheric pressures.

A. Key Equations

The current, I , delivered by a fission chamber is given by (see [1]):

$$I = e \iiint_V (N(r) - kn_e n_a + \alpha(E) n_e v_e) dV \quad (1)$$

where V is the inter-electrode volume. The parameters involved in the integral obey to a system of nonlinear differential equations [2]:

$$\begin{cases} \text{div}(n_e \underline{v}_e) = N(r) - kn_e n_a + \alpha(E) n_e v_e \\ \text{div}(n_a \underline{v}_a) = N(r) - kn_e n_a + \alpha(E) n_e v_e \\ \text{div}(\underline{E}) = e(n_a - n_e) / \epsilon_0 \epsilon_R \end{cases} \quad (2)$$

The first two equations describe the electric charge conservation; the last one is the Maxwell-Gauss formula. In (2), n_a and n_e are, respectively, the ion and electron densities; v_a and v_e are their drift speeds in the filling gas. N is the density of electron-ion pairs created per unit of time by the fission products in the detector. \underline{E} is the electric field generated between the detector electrodes. The $\alpha n_e v_e$ term results from the secondary ionizations induced by fast electrons, with α being the Townsend first ionization coefficient. At the opposite, the $kn_e n_a$ term represents the charge losses due to the electron - ion volumic recombinations, with k being the recombination coefficient.

Three boundary conditions complete (2): (a) the electronic density is null at the cathode surface, (b) the ionic density is null at the anode surface, (c) a voltage, ΔV , being applied between anode and cathode for charge collection, we have:

$$\int_L \underline{E} \cdot d\underline{l} = \Delta V \quad (3)$$

where L is any possible path linking the anode to the cathode.

Using a perturbation method, we obtained analytical solutions for (2) with boundary conditions (a) to (c). The corresponding results, gathered in [2] - [4], are used in this paper for the fission chamber modelling.

B. Parameters of the Modelling

In [1] and [5], we established that the density N can be approached, in cylindrical geometry, by:

$$N(r, z) \approx \frac{\tau_f X_0}{4\pi^2 h} \int_{\theta' = -\arccos(R_1/r)}^{\arccos(R_1/r)} \int_{z' = -h/2}^{h/2} \frac{dz' d\theta'}{R_1^2 + r^2 - 2rR_1 \cos(\theta') + (z - z')^2} \quad (4)$$

where R_1 and h are, respectively, the anode radius and length. r and z are the cylindrical coordinates (see Fig. 1). τ_f is the fission rate, i.e. the number of fissions occurring per unit of time in the fissile deposit. X is the mean number of electron - ion pairs created by the fission products per unit of length travelled in the gas. For micro detectors, the inter-electrode gap is small, thus X is constant, equal to X_0 [5]. Approximate values of X_0 for inert gases are gathered in Table 1.

When the distance $r - R_1$ is small compared to h , N can be well approached by (see [5]):

$$N(r, z) \approx \frac{\tau_f X_0}{2\pi h} \frac{1}{r} \times K\left(\frac{R_1}{r}\right) \times \Theta\left[-\frac{h}{2} \leq z \leq \frac{h}{2}\right] \quad (5)$$

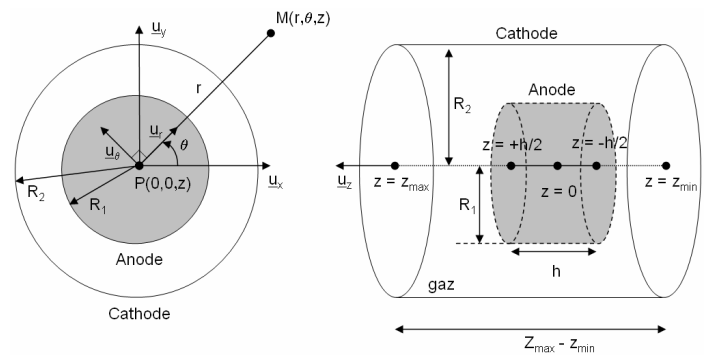


Fig. 1. Schematic view of a cylindrical fission chamber.

where Θ is a step function, equal to 1 when $-h/2 \leq z \leq h/2$ and null outside. The function K is the complete elliptic integral of the first kind [6].

Using (1) and (5), we obtain the saturation current, I_{sat} , of the detector, given in [5], [7] - [8]:

$$I_{sat} = e\tau_f X_0 \left[R_2 \times E\left(\frac{R_1}{R_2}\right) - R_1 \right] \quad \text{when } \frac{R_2 - R_1}{h} \ll 1 \quad (6)$$

where the function E is the complete elliptic integral of the second kind [6].

The diffusion contribution to the charge velocities becomes rapidly negligible in comparison with the electric field contribution. Thus, the charge speeds, v_e and v_a , can be written:

$$\underline{v}_e = -\mu_e \underline{E}, \quad \underline{v}_a = \mu_a \underline{E} \quad (7)$$

where μ_e and μ_a are the electron and ion mobilities. Approximate values for μ_e and μ_a are given in Table 1 for rare gases [9].

TABLE I
IONIZATION PARAMETERS FOR RARE GASES

Gas	X_0/P	$\mu_e \times P$	$\mu_a \times P$	A	B
Helium	$2.32 \cdot 10^7$	0.259	$3.3 \cdot 10^{-4}$	\times	\times
Neon	$7.99 \cdot 10^7$	0.086	$1.1 \cdot 10^{-4}$	\times	\times
Argon	$1.80 \cdot 10^8$	0.035	$4.4 \cdot 10^{-5}$	$1.19 \cdot 10^5$	$3.12 \cdot 10^6$
Krypton	$2.70 \cdot 10^8$	0.020	$2.6 \cdot 10^{-5}$	$3.97 \cdot 10^4$	$4.77 \cdot 10^6$

X_0/P is given in $\text{m}^{-1} \cdot \text{bar}^{-1}$ [9]

$\mu_e \cdot P$ and $\mu_a \cdot P$ are given in $\text{m}^2 \cdot \text{V}^{-1} \cdot \text{s}^{-1} \cdot \text{bar}$ [9]

A is given in $\text{m}^{-1} \cdot \text{bar}^{-1}$

B is given in $\text{V} \cdot \text{m}^{-1} \cdot \text{bar}^{-1}$

The Townsend coefficient, α , can be evaluated through calculations involving BOLSIG software [10] (see Fig. 2). For argon and krypton, we note that α can be well approached by the classical formula:

$$\frac{\alpha}{P} \approx A e^{\frac{BP}{E}} \quad (8)$$

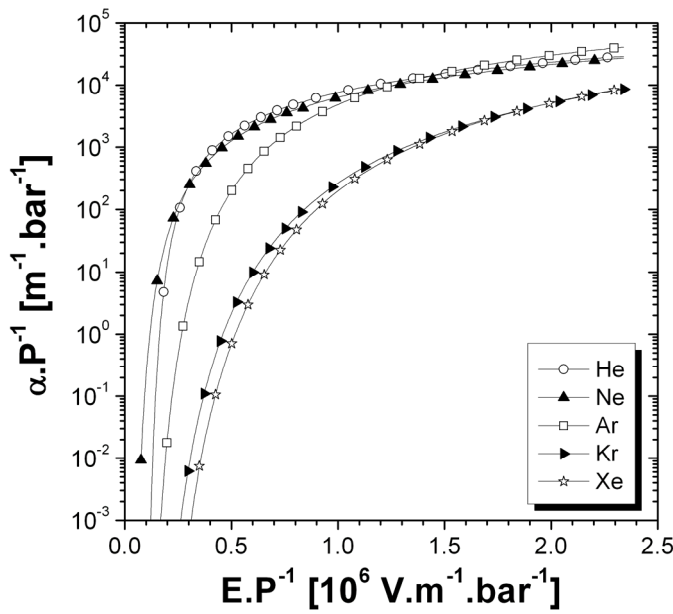


Fig. 2. Townsend first ionization coefficient, α , for rare gases.

where P is the pressure of the filling gas. Parameters A and B given in Table 1 are obtained fitting Fig. 2 results with (8).

The estimation of the recombination coefficient, k , is more difficult, as it exists very few experimental data in the literature, and none, at our knowledge, for inert gases at atmospheric pressures. This lack of data constitutes one of the major constraints for the fission chamber modelling, and should appreciably be completed through dedicated experiments. Nevertheless, k can be roughly approached by Langevin formula:

$$k \approx \frac{e(\mu_e + \mu_a)}{\varepsilon_0 \varepsilon_R} \quad (9)$$

where ε_0 is the void permittivity and $\varepsilon_R \approx 1$, the relative permittivity of the gas. Note however that experiments conducted at very low (\sim several Thor) or high (~ 100 bar) pressures showed that expression (9) strongly overestimates the recombination coefficient [11] – [12]. Note also that, as we demonstrated it in [2], the perturbations induced by the space charges on calibration curves can be neglected only when the Langevin factor, $\lambda = e(\mu_e + \mu_a)/k\varepsilon_0\varepsilon_R$, of the filling gas is close to 1. Consequently, if (9) overestimates k , then it means that the space charges must be accounted for in fission chambers operated in current mode, thus justifying the introduction of the Maxwell-Gauss equation in (2).

III. OPTIMIZING THE WIDTH OF THE SATURATION REGIME

Neutron flux measurements with fission chambers operated in current mode require a precise determination of their saturation currents. The achievable precision is closely dependent on the voltage extension, L , of the saturation plateau. The larger it is, the smaller the error bars on the flux values will be; consequently we propose in this section to

estimate it, and predict its evolution with parameters such as the electrode radii or the filling gas nature.

This study takes on great importance at high neutron fluxes, as deformations of the saturation curves occur, leading progressively to the complete disappearance of the saturation regime and resulting thus in an indeterminate of the flux [1].

A. Lower Limit of the Saturation Regime

The voltage ΔV_{min} , which tags the transition between the recombination regime and the saturation plateau, can be approached solving (2) with $\alpha = 0$ (secondary ionizations

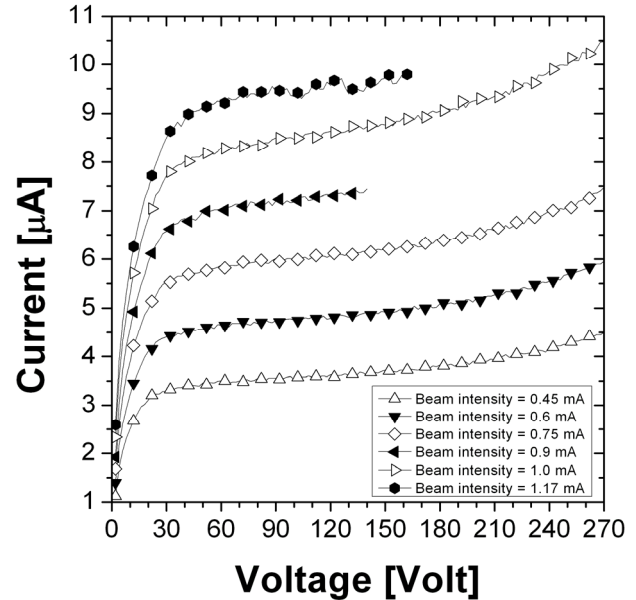


Fig. 3. Experimental calibration curves obtained for increasing neutron fluxes (CFUT-C3 chamber, $P = 1$ bar, $R_1 = 1.25$ mm, $R_2 = 1.75$ mm, filling gas = argon, fissile deposit = pure ^{235}U).

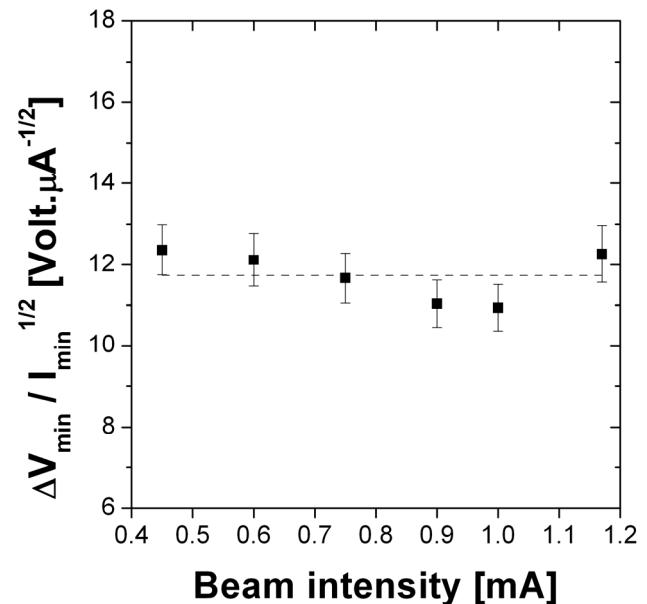


Fig. 4. Test of (10) for different neutron fluxes.

neglected as they occur at high voltages). It obeys to the equation $I_{min} = 0.95 \times I_{sat} = f(\Delta V_{min})$. Using perturbation methods completed with numerical resolutions of (2) (see [2]), we show that ΔV_{min} can be approached by:

$$\begin{aligned} \Delta V_{min} &\approx 0.87 \times (1 + \varepsilon(\lambda_e, \lambda_a)) \times (R_2^2 - R_1^2) \ln\left(\frac{R_2}{R_1}\right) \sqrt{\frac{k\langle N \rangle}{\mu_e \mu_a}} \\ &\approx 0.5 \times (1 + \varepsilon(\lambda_e, \lambda_a)) \times \ln\left(\frac{R_2}{R_1}\right) \sqrt{\frac{kI_{sat}(R_2^2 - R_1^2)}{\mu_e \mu_a e h}} \end{aligned} \quad (10)$$

where I_{sat} is the saturation current of the detector, h the anode length and e the elementary charge. The coefficients λ_e and λ_a are the electronic and ionic Langevin factors of the filling gas,

introduced in [2]. The factor ε appearing in (10) is a function of λ_e and λ_a . It represents the impact of the space charges on the current delivered by the detector. Values of ε are gathered in [2].

In Fig. 3, we present experimental calibration curves obtained with a Photonis CFUT-C3 fission chamber, irradiated inside the central rod of the MEGAPIE spallation target (distance to the target window: 370 mm), for increasing proton beam intensities [13] (and thus increasing neutron fluxes). In Fig. 4, we verify that the ratio $\Delta V_{min}/I_{min}$ is a constant, as predicted by (10). To obtain ΔV_{min} , we adjusted the saturation plateaux of Fig. 3 calibration curves with a linear fit $I = A \cdot \Delta V + B$, in order to suppress the perturbations due to cable resistances or secondary ionization reactions. We then posed $I_{min} = 0.95 \times B$.

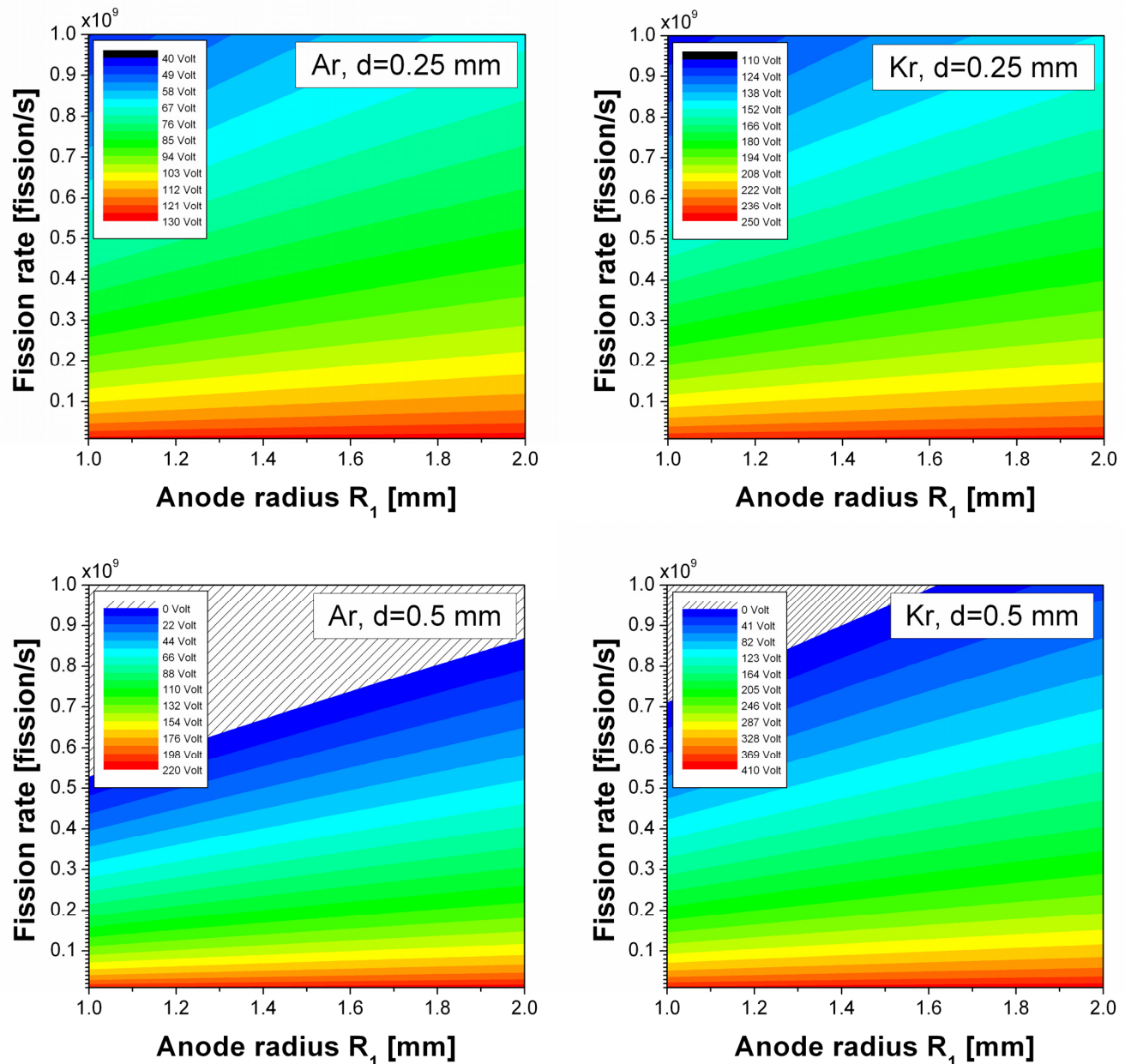


Fig. 5. Voltage extension, $L = \Delta V_{max} - \Delta V_{min}$, of the saturation regime for argon and krypton, as function of the anode radius, R_1 , the fission rate, τ_f , and the inter-electrode gap, $d = R_2 - R_1$ ($P = 1$ bar).

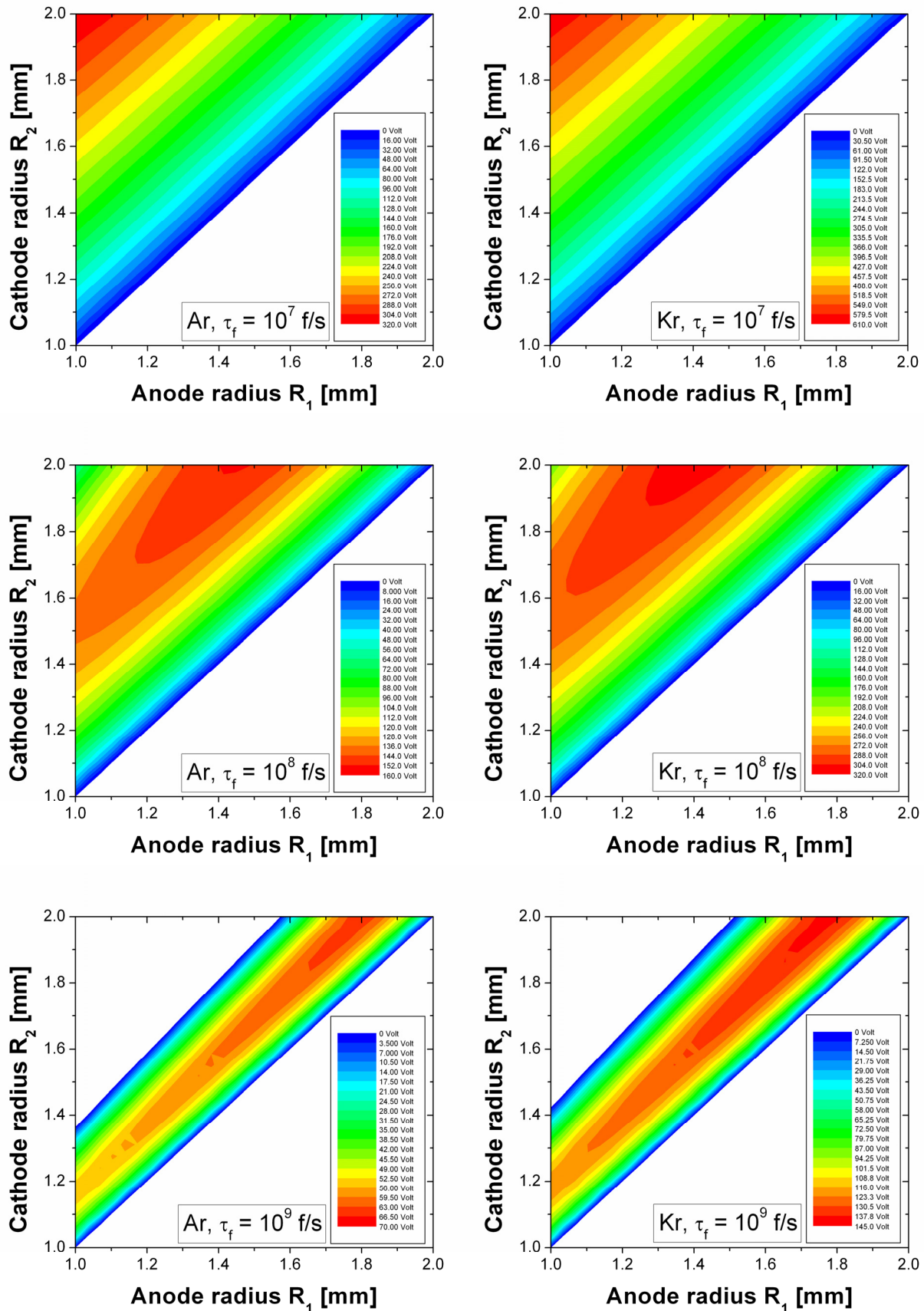


Fig. 6. Voltage extension, $L = \Delta V_{max} - \Delta V_{min}$, of the saturation regime for argon and krypton, as function of the electrode radii, R_1 and R_2 , and the fission rate τ ($P = 1$ bar)

B. Upper Limit of the Saturation Regime

The voltage ΔV_{max} , which delimits the saturation plateau and the avalanche regime, is given by $I_{max} = 1.05 \times I_{sat} = f(\Delta V_{max})$. It can be obtained resolving (2) with $k = 0$ (recombination processes neglected as they occur at low voltages). For detectors with an inter-electrode gap small compared to the anode radius, we demonstrated in [1] that ΔV_{max} obeys to the following equation:

$$\alpha \left(\frac{\Delta V_{max}}{R_2 - R_1} \right) \approx \frac{0.098}{R_2 - R_1} \quad (11)$$

where R_1 and R_2 are the electrode radii. α is the Townsend first ionization coefficient, introduced in section 2. For argon and krypton, (8) and (11) lead to:

$$\Delta V_{max} \approx \frac{BP(R_2 - R_1)}{\ln(AP(R_2 - R_1)) + 2.323} \quad (12)$$

C. Voltage Extension of the Saturation Regime

The voltage extension of the saturation regime is directly given by the difference $L = \Delta V_{max} - \Delta V_{min}$. In Fig. 5 and 6, we present the evolution of L with the electrode radii and the fission rate, for two filling gases, argon and krypton, at atmospheric pressure. In absence of available experimental results for the recombination coefficient, we chose arbitrarily $k = 10^{-12} \text{ m}^3 \cdot \text{s}^{-1}$ at $P = 1$ bar, a number in the order of magnitude of the value proposed in [1] (after correction of the 4π error in formula (2.37) of the paper). With the mobilities given in Table 1 and results of [2], we obtain $\lambda_e/\lambda_a = 795$, $\lambda = 634$ and $\varepsilon = 5.8$ at $P = 1$ bar. According to (9), the recombination coefficient should be proportional to the mobilities, which imply for krypton: $k = 5.7 \cdot 10^{-13} \text{ m}^3 \cdot \text{s}^{-1}$, $\lambda_e/\lambda_a = 769$, $\lambda = 634$ and $\varepsilon = 5.8$ at 1 bar.

Considering the results presented in Fig. 5 and 6, we note that krypton could present far better characteristics than the usual argon for maximising the voltage extension of the saturation regime. Consequently, if experiments confirm these theoretical predictions, we recommend its use for miniaturized detectors operated in current mode. Calculations in progress, involving also xenon, show that this gas could even overtop krypton in some irradiation conditions. In Fig. 5 and 6, we finally note that, as observed experimentally, the saturation plateau can disappear at high fission rates if the electrode radii are not carefully optimized.

IV. CONCLUSION

Resolving the charge propagation equations, we estimate the voltage extension of the saturation regime for fission chambers operated in current mode. We show that the saturation plateaux of these detectors can disappear at high neutron fluxes if the characteristics of their filling gas and electrodes are not previously optimized. In particular, we demonstrate that the use of heavy rare gases, krypton and xenon, instead of the usual argon can greatly enhance the

width of the saturation zone. As a result, krypton/xenon filled chambers could operate correctly at higher flux levels than conventional argon filled detectors.

To enhance the predictability of fission chamber models, we note that measurements of the electron-ion recombination coefficient for rare gases at atmospheric pressures are strongly needed. In the literature, data exists at very low or very high pressures, but too few however at the intermediate values. Finally, these measurements should be completed by investigations on the impact initial recombination processes could have on the value of the voltage needed to reach saturation. Experimental and theoretical contributions on this field could help improving fission chamber models.

REFERENCES

- [1] S. P. Chabod et al., Nucl. Instr. and Meth. A 566 (2006) 633
- [2] S. P. Chabod, Nucl. Instr. and Meth. A 602 (2009) 574
- [3] S. P. Chabod, Nucl. Instr. and Meth. A 595 (2008) 419
- [4] S. P. Chabod, Nucl. Instr. and Meth. A 604 (2009) 632
- [5] S. P. Chabod et al., Nucl. Instr. and Meth. A 598 (2009) 578
- [6] I. S. Gradshteyn, I. M. Ryzhik, Table of integrals, series, and products, fifth ed., Academic Press, Inc., 1965
- [7] L. Oriol et al, In-pile CFUZ53 sub-miniature fission chambers qualification in BR2 under PWR condition, Proc. Joint TRTR-IGORR Meeting, Gaithersburg, MD, USA, Sept. 12-16 2005, 2006. Available: <http://www.ncnr.nist.gov/trtr2005/Proceedings/Oriol - CFUZ53 Fission Chamber.pdf>
- [8] L. Vermeeren et al., In-pile sub-miniature fission chamber testing in BR2, Proc. 11th Symp. on Reactor Dosimetry, Brussels, Belgium, Aug. 18-23 2002, eds. J. Wagemans et al., World Scientific, 2003, pp 364
- [9] S. P. Chabod, Development and modelling of fission chambers designed for high neutron fluxes, applications at the HFR reactor (ILL) and the MEGAPIE target (PSI), PhD thesis, Paris XI (2006), available: <http://www-ist.cea.fr/publiccea/exl-doc/200700001303.pdf>
- [10] Available in freeware: www.siglo-kinema.com
- [11] K. Shinsaka et al, J. Chem. Phys. 88 (12) (1988).
- [12] M. A. Biondi, Phys. Rev. 129 3 1181-1188 (1963)
- [13] S. P. Chabod et al., Nucl. Instr. Meth. A 562 (2006) 618